



Design and Experimentation of a Novel Separable Vibration-Assisted Stage

Bowen Song¹ · Xiubing Jing¹ · Yingying Ren¹ · Yongqin Ren² · Huaizhong Li³

Received: 15 March 2023 / Revised: 5 May 2023 / Accepted: 7 May 2023
© The Author(s) 2023

Abstract

In this paper, a novel, separable two-degrees-of-freedom stage with high-precision motion and resolution is proposed for the application of vibration-assisted micromilling. A separable design was realized on the basis of the detachable structure of the platform. Flexible stages with different dimensions and types can be utilized in the devices. A circular-fillet hinge is selected as the flexible unit with a parallel structure to realize output decoupling and reduce the coupling error between the two vibration directions. Analytical modeling is conducted to explore the static and dynamic characteristics of the stage. Results reveal a good agreement with the finite element simulation result. A series of experiments were conducted to assess the static and dynamic performances of the flexible stage, encompassing tests such as amplitude response, motion trajectory, and coupling trajectory. The results of these tests revealed that the designed vibration-assisted system exhibits precise movement capabilities.

Highlights

- A novel separable vibration-assisted stage with high-precision motion and resolution is proposed, in which flexible stages with different dimensions and sizes can be utilized.
- The test results show that the coupling error of the 1D stage is much lower than the 2D stage in one-direction vibration.
- A motion trajectory test was performed to evaluate the 2D vibration precision of the stage, and an elliptical trajectory with a maximum error of 0.21 μm was obtained.

Keywords Vibration-assisted machining · Micromilling · Symmetrically decoupling structure · Flexible stage

✉ Xiubing Jing
jingxiuping@tju.edu.cn

✉ Yongqin Ren
101033293@qq.com

¹ School of Mechanical Engineering, Tianjin University, Tianjin 300354, China

² Key Laboratory of Ocean Observation Technology, Tianjin 300000, China

³ Griffith School of Engineering, Gold Coast Campus, Griffith University, Southport, QLD 4222, Australia

1 Introduction

Owing to the rapid development of the modern manufacturing process, micromilling has received considerable research attention within the fields of microelectromechanical systems (MEMS), biomedical engineering, aerospace, and other industries due to its high machining efficiency, fabrication accuracy, and low processing cost [1]. Recent studies have demonstrated that applying external energy, such as high-frequency vibration, to the machining process reduces the cutting force, improves machining precision, and suppresses surface damage [2]. This method is referred to as vibration-assisted machining (VAM). The periodic separation between

a tool and workpiece can be achieved, which can reduce the cutting heat and remove burs, resulting in smooth surface generation and low temperature [3].

VAM, originally designed to enhance the machinability of difficult-to-machine materials, has recently demonstrated its capability to generate surface textures [4]. Engineered textured surfaces feature a regular texture structure, which allows the component surface to possess superior attributes, such as reduced adhesion friction, improved lubricity, increased wear resistance, varied hydrophilic performance, and enhanced optical properties [5]. MEMS technology, energy beam processing technology, electrical discharge machining, and ultraprecision machining technologies can be used in microsurface texture manufacturing. However, these technologies are limited in their applicability, as they require long fabrication periods for large surface areas and certain materials. VAM has gained extensive attention due to its low cost, high efficiency, and environmental protection [6].

VAM can generally be implemented in two ways: applying vibration to the tool and the workpiece. The milling cutter typically revolves at an extremely high speed during the milling process; thus, the second method of delivering vibration to the workpiece is generally available for the subsequent design. Constructing a flexible stage is necessary to fix the workpiece to implement the aforementioned method. A piezoelectric actuator (PZT) is frequently utilized as a high-frequency excitation source to facilitate the flexible stage during the VAM process. Moreover, considering the PZT operating frequency, VAM can be classified as resonance or non-resonance VAM [7]. Resonance and non-resonance VAM both have advantages and limitations [8]. The resonance VAM can achieve efficient vibration with a large motion displacement. However, its vibration frequency is also fixed around the resonant frequency. The non-resonance VAM can achieve a flexible section of the vibration frequency [9]. However, low vibration efficiency and motion displacement restrict this approach in certain fields [10].

VAM can be commonly classified into three types corresponding to the direction of vibration: 1D, 2D, and 3D VAM. In a 1D VAM, vibration is delivered in either the feed or crossfeed direction, facilitating the movement of the workpiece in a single direction. In 2D VAM, vibration co-occurs in the feed and crossfeed directions, causing an elliptical motion of the workpiece in a plane. Furthermore, in a 3D VAM, the vibration is applied perpendicular to the machining plane, leading to a space ellipse trajectory in the cutting process. Correspondingly, the vibration stages can be classified into 1D, 2D, and 3D stages. 1D VAM can be realized in the 2D and 3D vibration stages; however, severe coupling errors will occur, considerably impacting movement accuracy.

Zhu et al. [11] presented a novel 2D vibration-assisted-compliant cutting system for conventional machines to generate textured surfaces with uniform and accurate topography. However, the method used in the cutting process is highly suitable for turning. Zheng et al. [12] suggested a new 2D PZT-driven vibration stage with a double-parallel four-bar linkage construction with double-layer flexible hinges to guide the motion and reduce displacement coupling between the two directions. However, the accuracy of the vibration stage may be impacted due to the vast size between the PZT and the stage. Börner et al. [13] proposed a 2D resonance VAM system in which the vibrator was designed in the shape of a cross, and the PZT was used to provide high-frequency vibration to the cross converter. The resonance frequency of the vibrator may be altered by enormous mass specimens. Ding et al. [14] described a 2D non-resonant vibration stage in which two pairs of PZTs were symmetrically distributed in flexible hinges around the mechanical oval structure, and a circuit board was integrated into the vibration stage to improve control accuracy. However, coupling error does exist and affects the motion accuracy due to the structural design.

Extensive research efforts have been devoted to designing the vibration stage. The authors believe that most vibration stages for VAM are integrated; therefore, only a single vibration type and performance can be supplied. Consequently, achieving efficient vibration for different requirements is considerably difficult. The separable design proposed in this paper could easily solve this problem. Furthermore, the worn stage could be replaced conveniently, which could reduce production costs and improve productivity.

In this study, the VAM platform is designed to be separable, which implies that the central stage can be replaced with different types, such as 1D and 2D stages with distinct sizes. Compared to the 2D vibration stage, the 1D stage possesses a large stiffness in the cross-vibration direction, which represents a small coupling error in the one-direction vibration application. Flexible applications can be obtained under various situations by changing stages with different types and vibration characteristics. In many cases, due to the limitations in the power and frequency of stacked piezoelectric ceramics, driving the flexible stage at the resonance frequency of the vibration stage is typically required to achieve efficient and reinforced vibrations.

This paper aims to provide a vibration-assisted platform with a separable design and high precision. Different types and dimensions of the stages could be used by applying the separable design approach to satisfy distinct operating requirements. A hybrid decoupling technique is proposed based on a circular-fillet hinge and parallel structure, which can simultaneously achieve high accuracy and output decoupling. The remainder of this article is structured as follows. Section 2 describes the mechanical design and operation of

the suggested vibration platform. Section 3 discusses finite element simulations and experimental tests. Finally, Sect. 4 presents the findings.

2 Mechanical Configuration

2.1 Structural Design

The basic structure of the proposed 2-DOF vibration-assisted platform, primarily comprising a pair of PZTs, a changeable flexible stage, and a support base, is illustrated in Fig. 1. The four corners of the flexible stage are positioned close to the support base to improve the accuracy of the assembly. The changeable flexible stage can be commonly divided into 1D and 2D stages, and their schematics are illustrated in Fig. 2. The main factors influencing the motion accuracy of a flexible stage include the coupling error, response hysteresis, and vibration. The coupling error can be defined as

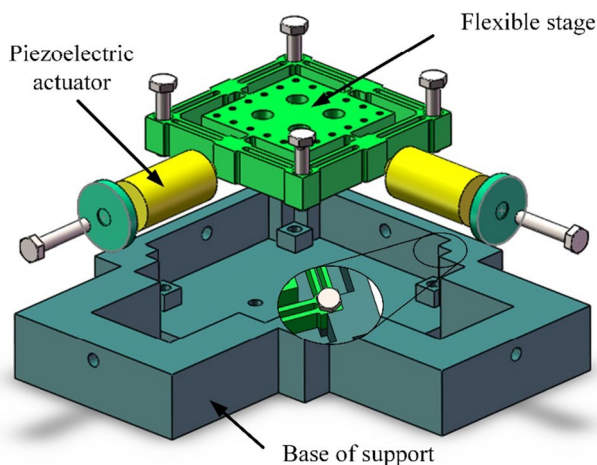


Fig. 1 Structure of the proposed separable vibration-assisted platform

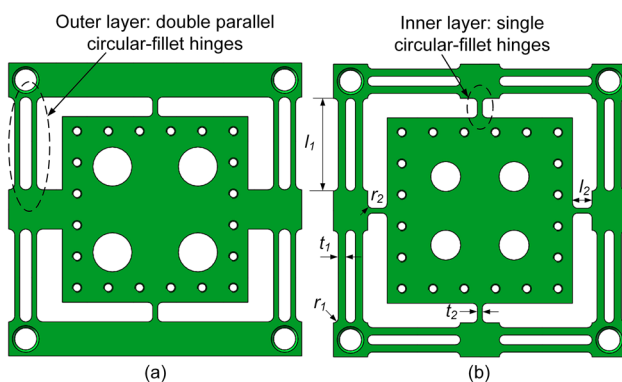


Fig. 2 Schematic of the **a** 1D and **b** 2D flexible stages

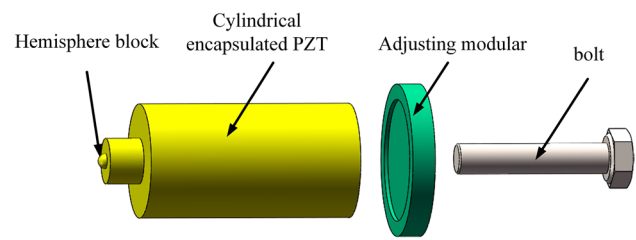


Fig. 3 Cylindrical-encapsulated PZT with its adjustment mechanism

the coupling displacement in directions other than the one corresponding to stage vibration, which considerably influences the vibration process [2]. The entire structure is symmetrically designed, and a two-layer mechanism is utilized in the two vibration directions to achieve two decoupling directions. The compression stiffness of the double-parallel flexure hinge is substantially higher than its rotational stiffness. Thus, a novel double-parallel flexure hinge is used as the outside framework of the stage to further reduce the coupling effect. The inner layer mechanism uses a single beam hinge to extend the vibration range of the mechanism. In addition, circular-fillet hinges are employed throughout the construction to increase the motion precision and reduce the stress concentration.

The necessary driving force in the VAM is relatively large in the current study. Therefore, stacked piezoelectric ceramics with excellent driving force performance were used in the experiment. The stacked piezoelectric ceramics have a limitation in the lower lateral torque bearing; thus, a PZT with a hemisphere block was selected to ensure protection from undesired shearing stress. The preloading force in the two directions must be identical; thus, cylindrical-encapsulated ceramics with a built-in preload were chosen. Meanwhile, the adjusting modular is designed and positioned between the bolt and PZT to restrict the vibration of PZT primarily in the horizontal direction. Figure 3 shows the cylindrical-encapsulated PZT with its adjustment mechanism, including the adjusting modular and bolt.

In the milling process, the resonant frequency and compliance are the most critical parameters because they are directly responsible for the vibration-assisted performance of the flexible stage. If the spindle speed is constant, the experimental frequency determines the amount of vibration assistance in one revolution. When the stage resonant frequency is used as the experimental frequency to improve the driving efficiency of piezoelectric ceramics, a high resonant frequency also implies increased vibration assistance in one milling revolution, which can improve the milling performance. Furthermore, the resonant frequency plays a crucial role in engineered textured surface machining. Simultaneously, the vibration displacement in

the vibration-assisted process was determined by compliance. If the driving force remains constant, then the high compliance indicates a highly substantial displacement. Minor vibration-assisted displacements will lead to an unclear experimental outcome. Other parameters such as mass, elastic modulus, and density, also affect the performance of the flexible stage; thus, their impacts are reflected in the resonant frequency and compliance. Therefore, these two factors must receive increased consideration during the flexible stage design.

2.2 Kinematic Analysis

The theoretical analysis of the vibration stage is of considerable importance to the analysis of static and dynamic characteristics. Multiple challenges can be addressed via theoretical analyses, such as calculating the compliance and natural frequency and determining the specific requirements for the PZT stiffness, output force, and stroke range. Several modeling methods, such as pseudo-rigid body, Castigliano’s second theorem, and finite element methods (FEMs), have been developed for flexible mechanism modeling. However, these methods have their applications and limitations. A matrix-based compliance modeling method built using the linear Hooke’s law for the material was recently developed. In the modeling process, the flexure hinge in the stage was uniformly divided into N pieces, with each piece being treated as a micro Euler–Bernoulli beam. High calculation accuracy and efficiency can easily be obtained by employing matrix operations. Thus, these operations are highly suitable for modeling spatial-compliant mechanisms with complex structures. Therefore, the matrix-based method was selected for modeling the proposed vibration stage. The compliance at the center point of the 2D flexible stage was the same in both directions due to the extreme symmetry design. Therefore, the stage can only be suitably

simplified in one direction for computing the compliance of the entire mechanism.

Figure 4a shows a simplified static analysis model of the stage in one direction, and Fig. 4b shows the element of the outer-hinge structure of the simplified model.

The two parallel circular-fillet hinges can be defined as a_1 and a_2 . Based on the matrix method, the outer compliance relative to the global coordinate C_{P_A} in Fig. 4b can be expressed as:

$$C_{P_A} = (k_{P_A})^{-1} = [(C_{a_1}^o)^{-1} + (C_{a_2}^o)^{-1}]^{-1} \tag{1}$$

where k_{P_A} is the outer stiffness relative to the global coordinates, and $C_{a_1}^o, C_{a_2}^o$ are the global compliance of hinges a_1 and a_2 relative to the stage center o-point, respectively. The local compliance C_i^r must be transferred from the local coordinate system $O_r - x_r, y_r, z_r$ to the global coordinate system $O_e - x_e, y_e, z_e$, as shown in Fig. 4c, to calculate the outer compliance C_r^e . The calculation formula is as follows:

$$C_r^e = T_r^e C_i^r (T_r^e)^T \tag{2}$$

where T_r^e is the coordinate transformation matrix and can be obtained according to Ref. [12].

Figure 4d shows the dimension and force analyses of the circular-fillet hinge. The hinge is assumed to be subjected to the force vector:

$$F = [F_x, F_y, F_z, M_x, M_y, M_z]^T, \tag{3}$$

where F_x, F_y, F_z and M_x, M_y, M_z are the forces and torques along the x -, y -, and z -axes, respectively. The corresponding deformation was defined as:

$$X = [\Delta_x, \Delta_y, \Delta_z, \alpha_x, \alpha_y, \alpha_z] \tag{4}$$

where $\Delta_x, \Delta_y, \Delta_z$ and $\alpha_x, \alpha_y, \alpha_z$ represent the displacements and torques along the direction of the x -, y -, and z -axes, respectively.

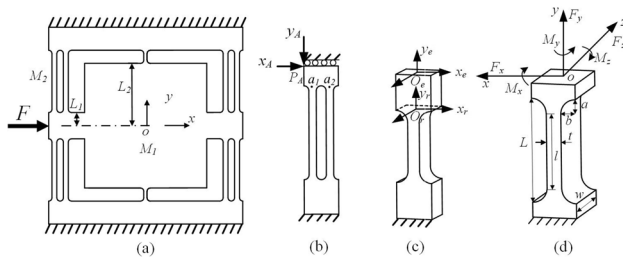


Fig. 4 **a** Static analysis model of the stage. **b** Element of the outer-hinge structure of the simplified model. **c** Transformation matrix. **d** Dimension and force analyses of the circular-fillet hinge

Table 1 Mechanical properties of 7075 aluminum

Material	7075 aluminum
Density	2.81 g/cm ³
Young’s modulus	71 GPa
Poisson’s ratio	0.33
Yield strength	455 MPa
Tensile strength	524 MPa

Considering the complex shear and torsion effects, the corresponding flexibility matrix C_h of each hinge is established to describe the yield strength. Therefore, the following relationship can be expressed as:

$$X = C_h F \tag{5}$$

Then, C_h could be calculated by:

$$C_h = \begin{Bmatrix} \frac{\Delta_x}{F_x} & 0 & 0 & 0 & 0 & 0 \\ 0 & \frac{\Delta_y}{F_y} & 0 & 0 & 0 & \frac{\Delta_z}{M_z} \\ 0 & 0 & \frac{\Delta_z}{F_z} & 0 & \frac{\Delta_x}{M_y} & 0 \\ 0 & 0 & 0 & \frac{\alpha_x}{M_x} & 0 & 0 \\ 0 & 0 & \frac{\alpha_y}{F_z} & 0 & \frac{\alpha_y}{M_y} & 0 \\ 0 & \frac{\alpha_z}{F_y} & 0 & 0 & 0 & \frac{\alpha_z}{M_z} \end{Bmatrix} \tag{6}$$

The compliance of the flexure hinge can be obtained in accordance with Ref. [15, 16]. The flexible stage is constructed using 7075 aluminum alloy, and its mechanical properties are outlined in Table 1.

The semi-inner structure contains only one flexure hinge due to the symmetrical design. The compliance of this structure corresponding to the local coordinate C_o^{in} is equal to its compliance $C_{m_1}^o$ corresponding to the global coordinate system $O_e - x_e y_e z_e$. The compliance matrix of the vibration stage in one direction C can generally be expressed as:

$$C = [(C_{P_A}/2)^{-1} + (C_{m_1}^o/2)^{-1} + (C_{P_A}/2)^{-1}]^{-1} \tag{7}$$

The dynamic analyses of the stage in each direction are identical due to the completely symmetrical design. Therefore, the unidirectional dynamics analysis discussion is sufficient. The equivalent stiffness of the flexure hinge in the X and Y directions is expressed in this model by k_{ix} and k_{iy} , respectively (i is the label of the flexure hinge; $i = a, b, c, \dots, m$). Suppose that the displacement under the action of force $F = [F_x, 0, 0]^T$ is $s = [x, 0, 0]^T$; the corresponding kinetic energy T_k and potential energy U_k can be respectively expressed as:

$$\begin{aligned} T_k &= \frac{1}{2} \dot{x}^2 M_1 + 4 \dot{x}^2 M_2 + 4 I_z \dot{\theta}_z^2 \\ U_k &= \frac{x^2}{2C} \end{aligned} \tag{8}$$

where M_1 and M_2 are equivalent masses of the hinge and center stage, respectively, and I_z and θ_z are the inertia moment and corresponding rotation angle of the flexure hinge around the Z -axis, respectively. By substituting the kinetic and potential energy into the Lagrange equation, the dynamic equation of the vibration stage can be obtained as follows:

$$\frac{d}{dt} \left(\frac{\partial T_k}{\partial \dot{x}} \right) - \frac{\partial T_k}{\partial x} + \frac{\partial U_k}{\partial x} = F_x \tag{9}$$

The dynamic equation describing the free motion of the stage can generally be expressed as follows:

$$\left(M_1 + 8M_2 + \frac{8I_z}{l^2} \right) \ddot{x} + \frac{x}{C} = F_x \tag{10}$$

where l is the hinge length.

The natural frequency of the vibration stage can then be obtained by:

$$\omega = \sqrt{\frac{1}{\left(M_2 + 8M_1 + \frac{8I_z}{l^2} \right) C}} \tag{11}$$

Finally, the theoretical compliance and the first natural frequency of the vibration stage can be calculated by Eqs. (7) and (11), respectively.

3 FEM Simulations and Experimental Tests

3.1 FEM Simulation

The FEM simulation of the vibration stage was conducted using the ANSYS Workbench 19.2. The meshing of the vibration stage is based on the hexahedron-dominated method, while the mesh refinement method was applied

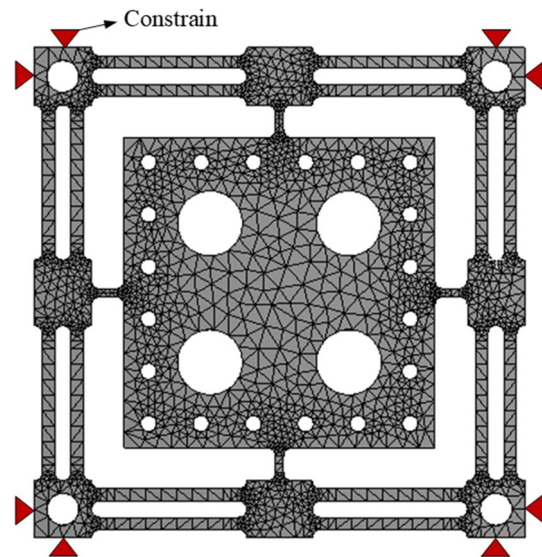


Fig. 5 Setup of the FEM model

Table 2 Key parameters of the structure

Parameters	Value (mm)
a	1
b	1
t	1.5
l	17
L_1	4
L_2	19

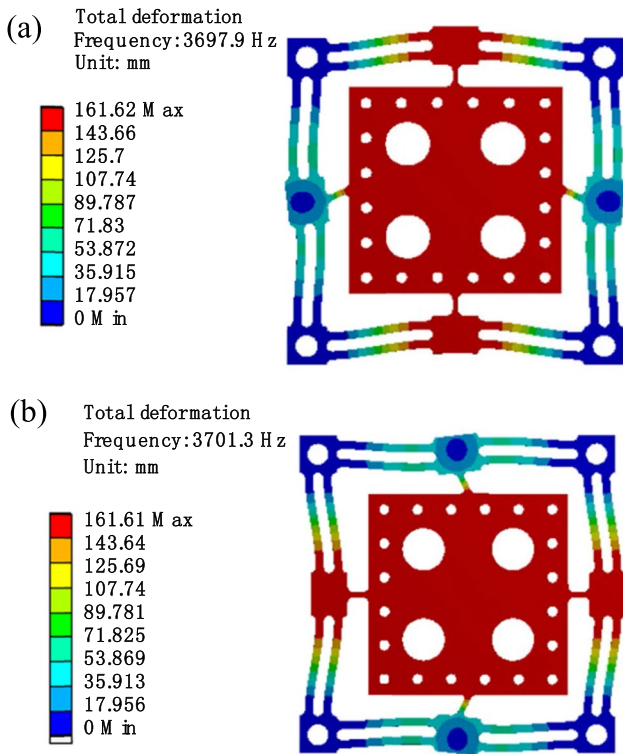


Fig. 6 First two resonance frequencies of the flexible stage: **a** first-order model and **b** second-order model

at the hinge connection. Figure 5 presents the FEM model setup of the vibration stage; the key parameters (as presented in Fig. 2) are given in Table 2. Considering the mode of the vibration stage in the prestressed state, the natural frequency and compliance of the vibration stage were obtained by constraining the four corner blocks. Figure 6 shows the first two resonance frequencies of the stage, which correspond to 3697.9 and 3701.3 Hz. The first- and second-order natural frequency shapes represent the translational motion of the vibration stage along the y - and x -axes, respectively.

Figure 7a shows that the axial displacement of the stage is $0.06373 \mu\text{m}$ for the case of the axial cutting force on the worktable at 1 N. Therefore, the axial stiffness and

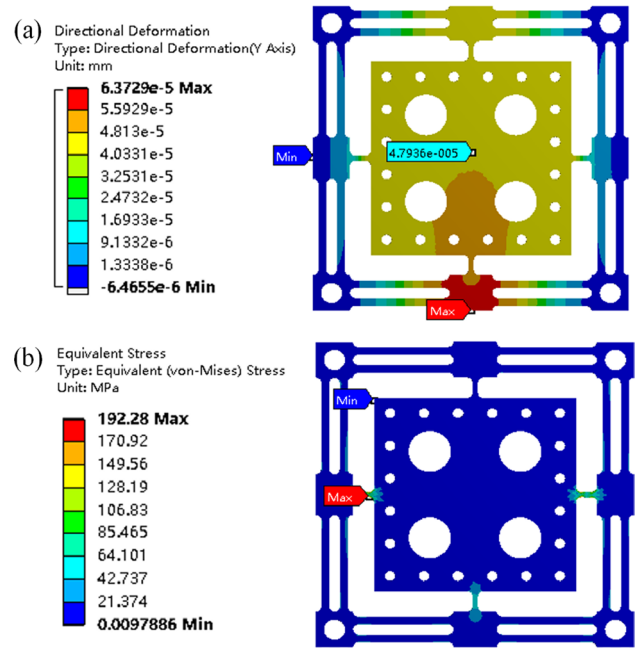


Fig. 7 Static simulation: **a** compliance simulation and **b** stress simulation

Table 3 Comparisons of the static and dynamic results corresponding to the flexible stage

Characteristics	Compliance	First natural frequency
Theoretical results	$0.0428 \mu\text{m/N}$	3915.6 Hz
FEM	$0.045 \mu\text{m/N}$	3697.9 Hz
Deviation	5.63%	5.15%

compliance of the stage are $20.86 \text{ N}/\mu\text{m}$ and $0.0479 \mu\text{m/N}$, respectively, which satisfies the actual machining requirements. Figure 7b shows the stress distribution in the vibration stage. The findings reveal that the maximum stress value is 192.28 MPa, which is substantially lower than the yield strength of the material (455 MPa).

Meanwhile, the theoretical calculation was also conducted with the key parameters shown in Table 2. The theoretical results were compared with that of the FEM simulation, as shown in Table 3.

The difference between the analytical model and FEM is within 10%, which indicates the excellent accuracy of the analytical model. Reasonably, the first natural frequency of FEM is slightly lower than that obtained from the theoretical results. The FEM considers every stage as flexible elements, while the theoretical method only considers the compliances of the flexible hinges in the vibration direction. Moreover, the compliances of the hinges in

cross-vibration, as well as structure M_1 shown in Fig. 4a, are completely ignored.

3.2 Experimental Tests

Figure 8a shows that the VAM stage is fixed on a precision three-axis micromilling machine. The support base comprised AISI 1045 steel to provide as much stiffness as possible. The 1D and 2D vibration stages, as respectively shown in Fig. 8b and c, were manufactured by utilizing an aluminum alloy 7075-T651. Ensuring a high natural frequency also provides considerable compliance. The two cylindrical-encapsulated PZTs are from CoreMorrow (PSt150/10/20 VS15 model). The driving signals were generated by the Agilent 33500B signal generator and further amplified by the piezoelectric control system (CoreMorrow’s E01.A2). A laser Doppler vibrometer was then fixed on the other side to monitor the real-time output displacement of the vibration stage. An NI 9221 input DAQ card was selected to collect the stage displacement data from the laser Doppler vibrometer, and the data were sent to the LabVIEW software for analysis.

A series of test experiments were designed and conducted to verify the performance and efficiency of the separable VAM system. By exerting a sinusoidal sweep voltage signal

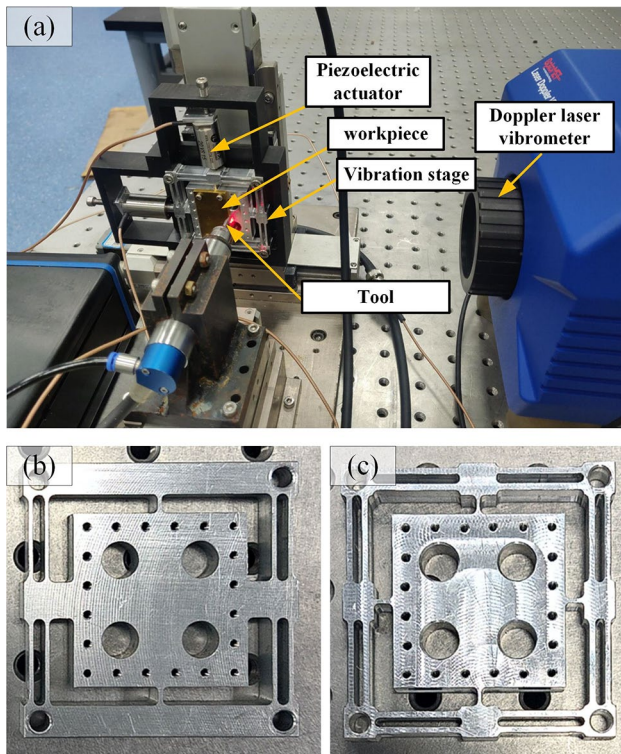


Fig. 8 a Experimental setup; b 1D vibration stage, and c 2D vibration stage

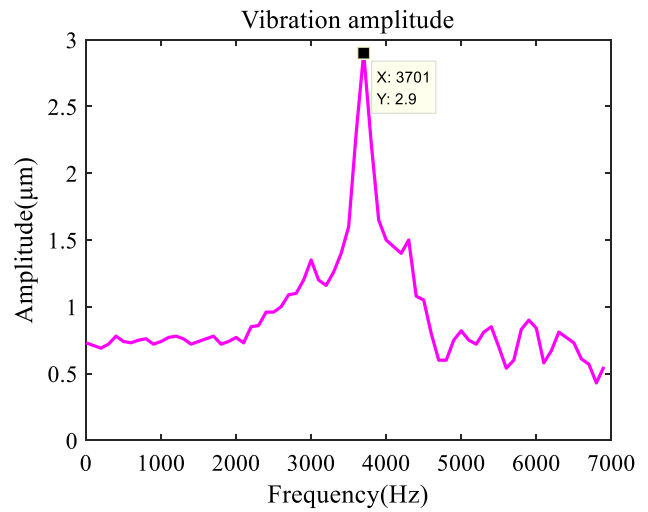


Fig. 9 Frequency amplitude results of the 2D flexible stage

of 15 V to the PZT at an interval of 100 Hz over the frequency range of 0–7000 Hz, the frequency amplitude results of the 2D flexible stage can be obtained as shown in Fig. 9. The frequency amplitude result shows that the natural frequency of the 2D stages is approximately 3700 Hz, which verified the simulation results.

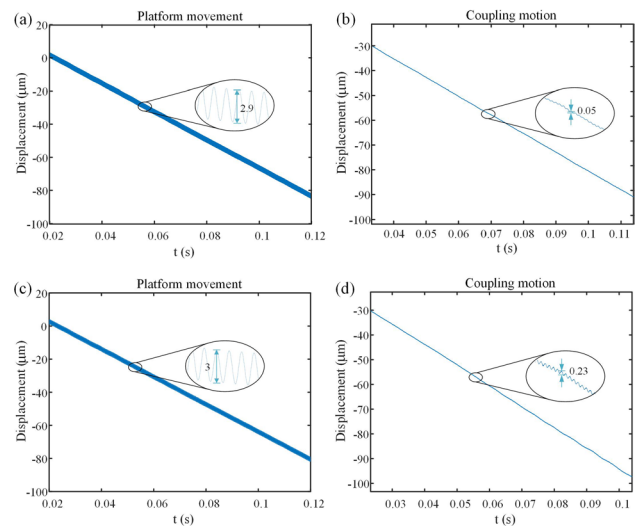


Fig. 10 Test results of 1D stage: a stage movement, b coupling motion; 2D stage: c stage movement, d coupling motion

Table 4 Comparisons of the coupling error between the 1D and 2D stages

Types	1D stage	2D stage
Vibration displacement (μm)	2.9	3
Coupling displacement (μm)	0.05	0.23
Coupling error	1.72%	7.67%

Moreover, the coupling displacement in one direction was tested with the application of vibration in the other direction to compare the coupling error between the 1D and 2D stages. The measuring range of the laser vibrometer was set to $100\ \mu\text{m}$ to ensure that the motion displacement of the guideway and the vibration displacement of the platform can be tested simultaneously. Figure 10a–d shows the stage displacement and coupling motion in the experimental process corresponding to the 1D and 2D stages, respectively. The test results are summarized as shown in Table 4, which presents the substantial low-coupling error performance of the 1D stage. Notably, the 1D vibration stage exhibits considerably large stiffness in the cross-vibration direction. Contrastingly, Zheng [12] used the PID (Proportional, Integral, Differential) control method to reduce the coupling displacement of the 2D stage from 0.25 to $0.15\ \mu\text{m}$, while the coupling error was controlled to within 2.6%, which is also higher than the 1D stage proposed in this paper. Meanwhile, the test results shown in Fig. 10 reveal the remarkable performance of the 1D and 2D stage during the application of large displacement. The motion displacements of the guideway and vibration stage do not impact each other, leading to the remarkable precision of composition displacement.

The VAM platform and test devices were arranged as shown in Fig. 11 to evaluate the coupling motion under the vibrations of two directions. Sinusoidal signals of 15 and 7.5 V were sent to the feed and crossfeed directions, respectively. Figure 12 shows the vibration displacement of the stage with 0° , 90° , and 180° vibration phase

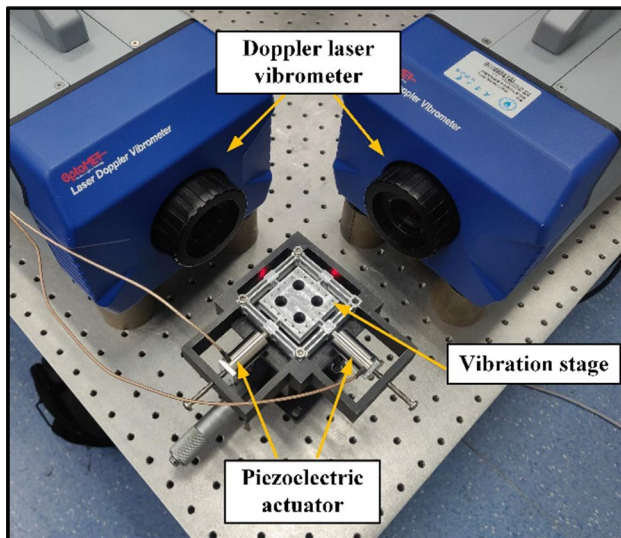


Fig. 11 Vibration motion trajectory test mechanism

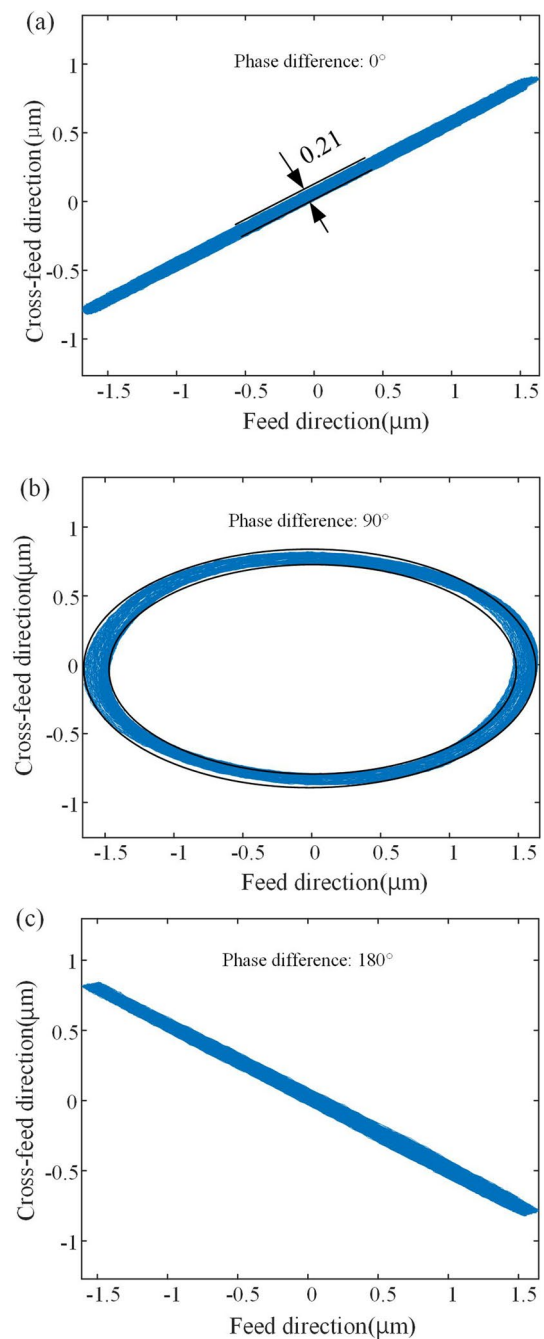


Fig. 12 Trajectory of the vibration stage with **a** phase difference of 0° , **b** phase difference of 90° , and **c** phase difference of 180°

differences. When the phase difference is 90° , an elliptical trajectory can be obtained by combining the vibration displacements of two directions, as shown in Fig. 12b. The total vibration trajectory errors (including the inherent

noise of the capacitive sensors) are 0.21 μm , signifying that the designed vibration-assisted system possesses precise movement capability.

4 Conclusions

A novel separable vibration-assisted platform was designed, analyzed, and tested for micromilling in the current study. A separable design can be realized on the basis of the detachable structure. 1D and 2D flexible stages were designed and utilized in the experiment, which adopted a two-layer mechanism with double-parallel fillet hinges to achieve high motion accuracy and reduce the coupling effect. The static and dynamic characteristics considering the designed flexible stage were obtained using theoretical analysis, FEM, and experimental tests, which formed a contrast verification. The coupling error of the 1D and 2D stages was tested and compared, and the results present a substantial low-coupling error performance of the 1D stage. A motion trajectory test was performed to evaluate the vibration precision of the stage, and an elliptical trajectory with a maximum error of 0.21 μm was obtained. The findings denote that the designed vibration-assisted system possesses precise movement capabilities.

Acknowledgements This research was supported by Program of Tianjin Science and Technology (No. 21ZXJBGX00020), and the National Natural Science Foundation of China (Nos. 51875404, 52175275).

Author Contributions All authors read and approved the final manuscript.

Data Availability Statement The data that support the findings of this study are available from the corresponding author upon reasonable request.

Declarations

Competing interest The authors declare that they have no competing interest.

Open Access This article is licensed under a Creative Commons Attribution 4.0 International License, which permits use, sharing, adaptation, distribution and reproduction in any medium or format, as long as you give appropriate credit to the original author(s) and the source, provide a link to the Creative Commons licence, and indicate if changes were made. The images or other third party material in this article are included in the article's Creative Commons licence, unless indicated otherwise in a credit line to the material. If material is not included in the article's Creative Commons licence and your intended use is not permitted by statutory regulation or exceeds the permitted use, you will need to obtain permission directly from the copyright holder. To view a copy of this licence, visit <http://creativecommons.org/licenses/by/4.0/>.

References

- Chen N, Li HN, Wu J, Li Z, Li L, Liu G, He N (2021) Advances in micro milling: from tool fabrication to process outcomes. *Int J Mach Tools Manuf* 160:103670. <https://doi.org/10.1016/j.ijmachtools.2020.103670>
- Zheng L, Chen W, Huo D (2020) Review of vibration devices for vibration-assisted machining. *Int J Adv Manuf Technol* 108(5–6):1631–1651. <https://doi.org/10.1007/s00170-020-05483-8>
- Zheng L, Chen W, Pozzi M, Teng X, Huo D (2019) Modulation of surface wettability by vibration assisted milling. *Precis Eng* 55:179–188. <https://doi.org/10.1016/j.precisioneng.2018.09.006>
- Yuan Y, Zhang D, Zhu H, Ehmann KF (2020) Machining of micro grayscale images on freeform surfaces by vibration-assisted cutting. *J Manuf Process* 58:660–667. <https://doi.org/10.1016/j.jmapro.2020.08.051>
- Gao W, Haitjema H, Fang FZ, Leach RK, Cheung CF (2019) On-machine and in-process surface metrology for precision manufacturing. *CIRP Ann* 68(2):843–866. <https://doi.org/10.1016/j.cirp.2019.05.005>
- Chen W, Zheng L, Huo D, Chen Y (2018) Surface texture formation by non-resonant vibration assisted micro milling. *J Micromech Microeng*. <https://doi.org/10.1088/1361-6439/aaa06f>
- Jin X, Xie B (2015) Experimental study on surface generation in vibration-assisted micro-milling of glass. *Int J Adv Manuf Tech* 81(1–4):507–512. <https://doi.org/10.1007/s00170-015-7211-2>
- Yuan Y, Zhang D, Jing X, Cao J, Ehmann KF (2019) Micro texture fabrication by a non-resonant vibration generator. *J Manuf Process* 45:732–745. <https://doi.org/10.1016/j.jmapro.2019.08.010>
- Chen X, Gu Y, Lin J, Yi A, Kang M, Cang X (2020) Study on subsurface damage and surface quality of silicon carbide ceramic induced by a novel non-resonant vibration-assisted roll-type polishing. *J Mater Process Technol* 282:116667. <https://doi.org/10.1016/j.jmatprotec.2020.116667>
- Liu Y, Liu ZB, Wang XB, Huang T (2021) Experimental study on cutting force and surface quality in ultrasonic vibration-assisted milling of C/SiC composites. *Int J Adv Manuf Tech* 112(7–8):2003–2014. <https://doi.org/10.1007/S00170-020-06355-X/FIGURES/14>
- Zhu WL, Zhu Z, He Y, Ehmann KF, Ju BF, Li S (2017) Development of a novel 2-D vibration-assisted compliant cutting system for surface texturing. *IEEE ASME Trans Mech* 22(4):1796–1806. <https://doi.org/10.1109/TMECH.2017.2693996>
- Zheng L, Chen W, Huo D, Lyu X (2020) Design, analysis, and control of a two-dimensional vibration device for vibration-assisted micromilling. *IEEE ASME Trans Mech* 25(3):1510–1518. <https://doi.org/10.1109/TMECH.2020.2978209>
- Börner R, Winkler S, Junge T, Titsch C, Schubert A, Drossel WG (2018) Generation of functional surfaces by using a simulation tool for surface prediction and micro structuring of cold-working steel with ultrasonic vibration assisted face milling. *J Mater Process Technol* 255:749–759. <https://doi.org/10.1016/j.jmatprotec.2018.01.027>
- Ding H, Chen SJ, Ibrahim R, Cheng K (2011) Investigation of the size effect on burr formation in two-dimensional vibration-assisted micro end milling. *Proc Inst Mech Eng B J Eng*. <https://doi.org/10.1177/0954405411400820>

15. Liu M, Wang W, Song H, Zhou S, Zhou W (2019) A high sensitivity FBG strain sensor based on flexible hinge. *Sensors*. <https://doi.org/10.3390/s19081931>
16. Zhao DM, Wang JW, Xu ZY (2021) Surface effect on vibration of Timoshenko nanobeam based on generalized differential quadrature method and molecular dynamics simulation. *Nanomanuf Metrol* 4:298–313. <https://doi.org/10.1007/s41871-021-00117-3>



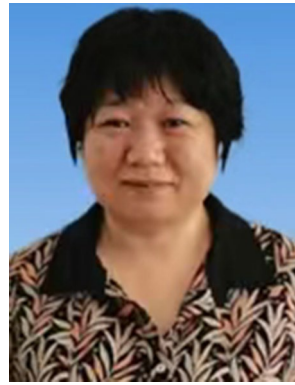
Bowen Song is a PhD candidate in mechanical engineering. He is pursuing a PhD in mechanical engineering at the School of Mechanical Engineering, Tianjin University. His current research interests include micro-scale manufacturing and vibration-assisted machining. He has published several papers in various reputed international journals, conferences, and proceedings.



Xiubing Jing received a PhD degree in mechanical engineering from Tianjin University, Tianjin, China. She is currently an associate professor at the School of Mechanical Engineering at Tianjin University. Her areas of research interests include mechanical dynamics, surface engineering, and micro/meso-scale manufacturing technology. She has published over 40 peer-reviewed technical papers in international journals and conference proceedings.



Yingying Ren is a ME candidate in mechanical engineering. She is pursuing a ME in mechanical engineering at the School of Mechanical Engineering, Tianjin University. Her current research interests include micro/nano machining and micro-machine tools for manufacturing of precision parts.



Yongqin Ren received a master's degree in optical engineering from Tianjin University. She is a senior engineer at the National Ocean Technology Center, Tianjin, China. She has been committed to designing, researching, and developing marine optical instruments. She has presided over and participated in several the national "863" Program and eleventh five-year projects, national key research and development projects.



Dr. Huaizhong Li obtained a PhD degree from the National University of Singapore. He is currently a Senior Lecturer at the School of Engineering and Built Environment, Griffith University, Australia. He is a Fellow of International Academy of Engineering and Technology (AET), Fellow of the Higher Education Academy (FHEA), and Fellow of the Griffith Learning and Teaching Academy. His research interests include advanced manufacturing technologies, micromachining, machine dynamics, vibration monitoring and control, and mechatronics.